JOURNAL OF AIRCRAFT
Vol. 29, No. 3, May–June 1992

Flow over a Twin-Tailed Aircraft at Angle of Attack Part I: Spatial Characteristics

N. M. Komerath,* S. G. Liou,† R. J. Schwartz,‡ and J. M. Kim‡
Georgia Institute of Technology, Atlanta, Georgia 30332

A quantitative study is reported on the low-speed flow environment of scale models of a twin-tailed fighter aircraft at high angles of attack. Laser sheet flow visualization is used to observe the various sources of vortex generation, and the evolution of these vortex flows. Surface tufts are used to observe the nature of flow separation on the vertical tails as angle of attack is varied. Laser Doppler velocimetry is used to quantify the time-averaged three-dimensional velocity field, and histograms of velocity, in selected planes proceeding from the inlets to the vertical tails. No concentrated vortex is observed near the vertical tails, however, the tails are seen to be immersed in a vortex flow of large radius. Flow separation propagates up the outside surfaces of the vertical tails, with increasing angle of attack; however, the flow on the inside surface of the tails remains largely attached. The flow angularity at the tails varies widely along the tail span, is sensitive to angle of attack, and fluctuates over a wide range at each location. These results are found to be relatively insensitive to the precise modeling of inlet through-flow and inlet attitude. Contours of the root-mean-square velocity fluctuations indicate that the largest fluctuations occur in the separated flow immediately above the wing surfaces.

Nomenclature

AR	=	wing aspect ratio
c_{av}	=	mean geometric chord
mac	=	mean aerodynamic chord
S	=	wing span
U_∞	=	freestream velocity
u	=	velocity component along freestream direction
u'	=	fluctuation about the mean value of u
v	=	velocity component along lateral direction
v'	=	fluctuation about the mean value of u
w	=	velocity component along vertical direction
w'	=	fluctuation about the mean value of w
X	=	distance along tunnel longitudinal axis
Y	=	distance along lateral axis
Z	=	distance along vertical axis
α	=	aircraft angle of attack
θ	=	flow angularity at the vertical tail
Λ	=	wing leading-edge sweep
λ	=	wing taper ratio
ω	=	x-component of vorticity

Introduction

COMBAT aircraft at high angles of attack experience unsteady vortex flows that cause problems such as tail buffeting[1,2] and the lateral instability.[3] The approach to such problems must be multifaceted, using results of wind-tunnel and flight tests to validate predictions,[4–7] for improved design. This paper describes an effort to define the low-speed, high-α aerodynamic environment of an F-15 aircraft as part of such a program.

Previous Work

Reference 8 summarizes an extensive program aimed at understanding and modifying the buffeting loads on the vertical tails of the F-15. Trajectories of streams of condensed water vapor were observed. Hot-wire anemometry and surface pressure measurements were conducted over a range of angles of attack. Flow angularity was measured upstream of the vertical tails. Vapor injected near the wing leading edge was seen to move inboard and impinge on the vertical tail. Wing fences and speed-brake deployment were used to deflect the vortex flow away from the tails. These were abandoned, because the fences caused adverse effects at other flight conditions and speed-brake deployment was not possible at all required flight conditions. Reference 1, conducted a few years later, reported surface tuft visualization and surface pressure measurements made with rigid and aeroelastically scaled vertical tails. Both of these studies are used here as points of reference.

It is only recently that fighter aircraft reached the stage where the time spent at high angles of attack became a substantial fraction of the total flying hours. Vibration-free control and long fatigue life under these conditions have become crucial issues, and emphasis on the twin-tail buffeting problem has increased. Sellers et al.[9] presented detailed measurements of the flow over a 3%-scale model of a YF-17. They showed the dominance of the leading-edge extension (LEX) vortices, and attributed the large velocity fluctuations (root-mean-square values of 30% of the mean) at the vertical tails to the bursting of these vortices. Zimmerman et al.[10] extended the work of Ref. 1 to the F/A-18, and developed a method for predicting tail buffet loads based on test data. They showed that buffet spectra could be extrapolated over large ranges of velocity, dynamic pressure, and model size, and that wind-tunnel data could be used to predict flight loads.

The problem of extrapolating model-scale data to flight tests has recently been reexamined in the context of high-α aerodynamics. Reference 11 compares vortex burst locations on the F/A-18 from experiments that span the range from1/48–scale models in water tunnels to actual flight tests. The correlation between model-scale tests and flight tests is surprisingly accurate. At large angles of attack, the flow separates quite close to the wing leading edge regardless of Reynolds number. Also, most high-α flight occurs at relatively low Mach numbers due to structural limitations. Thus, the effects of compressibility, although present, are not primary. Reference 12 shows some discrepancies between data obtained at different Reynolds and Mach numbers, showing that the effects of surface roughness, freestream turbulence, tunnel wall ef-

Received Oct. 24, 1990; revision received May 21, 1991; accepted for publication May 21, 1991.

*Associate Professor, School of Aerospace Engineering. Senior Member AIAA.
†Postdoctoral Fellow, School of Aerospace Engineering. Member AIAA.
‡Graduate Research Assistant, School of Aerospace Engineering. Student Member AIAA.

fects, and model support interference must be considered in each study. Schrader et al.[13] showed the formation of supersonic regions in the vortex flow above a delta wing at a freestream Mach number of 0.8. These regions were terminated through shocks oriented at shallow angles to the freestream. The forces and moments on control surfaces immersed in transonic vortex flows can, thus, be expected to be influenced by the occurrence of local supersonic flow.

Edwards[14] studied the magnitude of resources required to compute the high angle-of-attack buffet environment. He concluded that new analytical models, providing a better physical understanding of the dominant phenomena, were required before the environment could be computed with the resources that would be available in the near future.

Present Scope and Objectives

This effort is aimed at defining the aerodynamic environment of an F-15 at high angles of attack, and identifying the dominant phenomena. A large amount of flight experience has been accumulated on this type of aircraft. However, quantitative flowfield data on the high-α flow environment, suitable for modeling of the flowfield, are quite scarce. The present authors were unable to locate any substantial database on the F-15 other than those reported in Refs. 1 and 8. These, then, provide logical points of reference for this investigation. As shown later, the flowfield is very different from that of the F/A-18, on which there is an increasing amount of quantitative data.

The work was performed in steps of increasing detail, going from a description of the flowfield based on steady laser sheet visualization, to the dynamics of surface tufts, and on to quantitative measurements of the velocity field using laser Doppler velocimetry. The effects of geometric modifications and approximations made in high-speed models are examined to provide guidance in designing high-speed wind-tunnel models to study high-α tail loads. The quantitative data thus obtained provide the basis for detailed examination of fluctuation spectra, and their genesis. Part II of this work, focusing on the velocity fluctuations, is reported in Ref. 15.

The purpose and utility of low-speed tests using small-scale models must be carefully defined, despite the encouraging comparisons with full-scale results quoted before. Reynolds number and surface roughness are very different from those of actual aircraft. The justification for such tests is fourfold. First, it is impractical to obtain extensive flowfield data from tests run in very large wind tunnels, or from cryogenic or high Mach number tunnels. Second, parametric variations can be performed efficiently using small-scale models in low-speed tunnels. Third, the geometry and Reynolds number of the wind-tunnel model can be accurately simulated in computational prediction tools, so that the multifaceted and detailed experimental results from low-speed experiments can be used to develop and validate these predictions. The validated methods can be used, along with limited flight data and high-speed tunnel data as check points, to predict the features of the full-scale flight environment. Finally, it is expensive to develop prediction methods based on finite-difference techniques for the solution of the Navier-Stokes equations, with typical run-times for full aircraft configurations running into dozens of hours on the fastest of current computers. The Reynolds number has a strong bearing on these run-times, because higher Reynolds numbers mean thinner shear layers and denser grids. Thus, low-Reynolds-number results are of distinct utility in the development and validation of these methods. The effects of compressibility are obviously out of reach in these tests; again, it can be argued that these are of secondary importance in the high-α maneuver regime of current fighter aircraft, when the sources of high-cycle unsteady loads are sought.

Facility and Measurement Techniques

The experiments are conducted at the John J. Harper Low-Speed Wind Tunnel at Georgia Institute of Technology. This

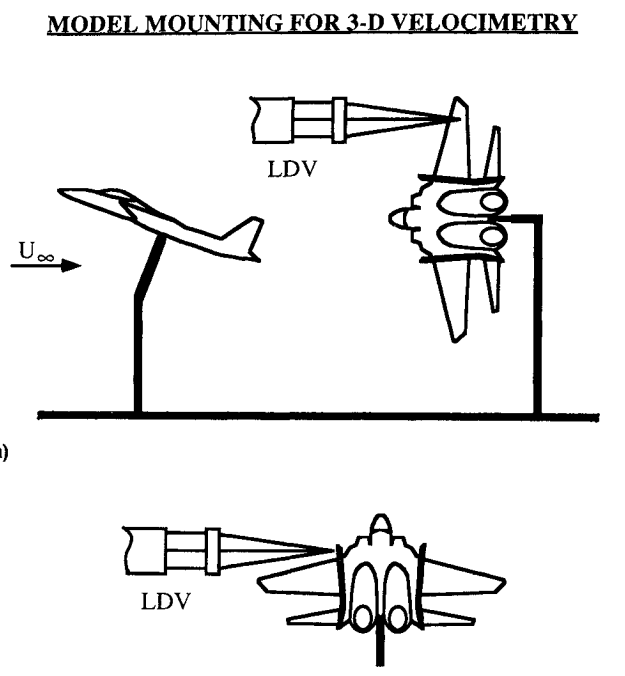

Fig. 1 Model mounting for laser velocimetry, showing method of measuring all three velocity components with a single-component laser velocimeter.

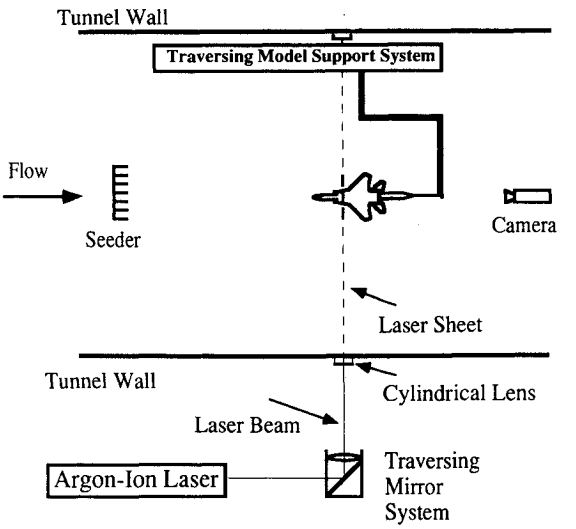

Fig. 2 Laser sheet flow visualization setup.

$\lambda = 0.25$	S = 0.4064 m
AR = 3.01	m.a.c = 0.1518 m
$\Lambda = 45^\circ$	c_{AV} = 0.1357 m

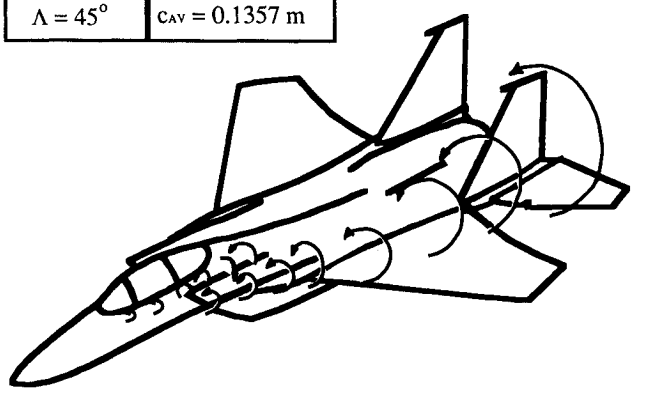

Fig. 3 Qualitative sketch of vortex flow features over an F-15.

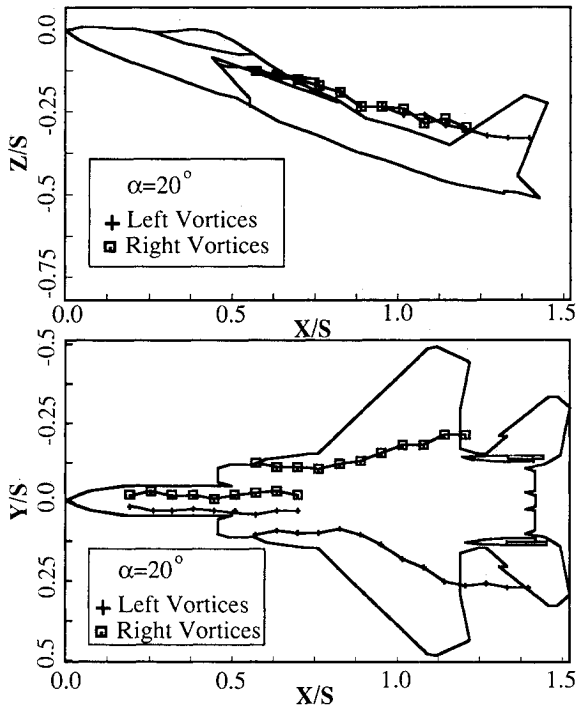

Fig. 4 Vortex trajectories at α = 20 deg, obtained by laser sheet visualization.

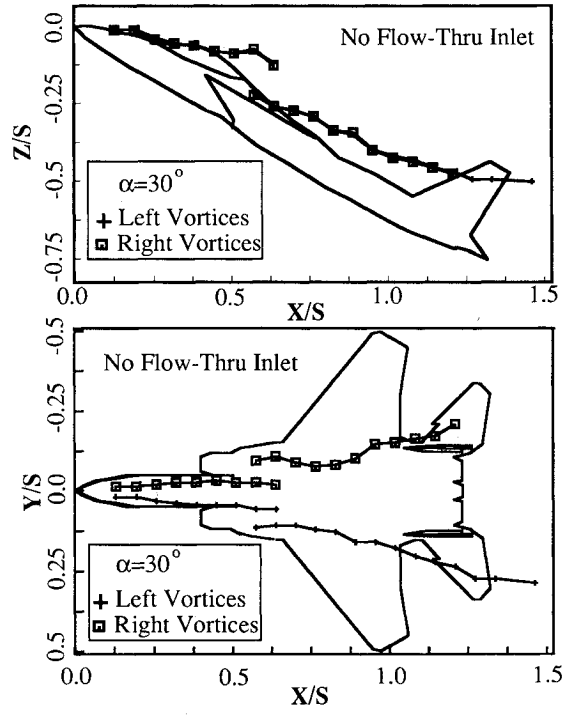

Fig. 5 Vortex trajectories at α = 30 deg, obtained by laser sheet visualization.

is a closed-return facility capable of speeds up to 73 m/s. The tunnel is powered by a 600-hp electric motor. The test section dimensions are 2.13 m × 2.74 m, being obtained using a flat floor and ceiling in a 2.74-m-diam circular section. Turbulence intensity is known to be under 0.5% over the speed range of interest.

The models used in these tests are of $\frac{1}{32}$-scale. A $\frac{1}{7}$-scale model was also built from a plexiglass kit to study surface tuft behavior and the frequency content of the velocity fluctuations. The external shape for the $\frac{1}{32}$-scale models is obtained using kits acquired from hobby shops. Steel spars and epoxy fillers are used to increase the strength and rigidity, and the

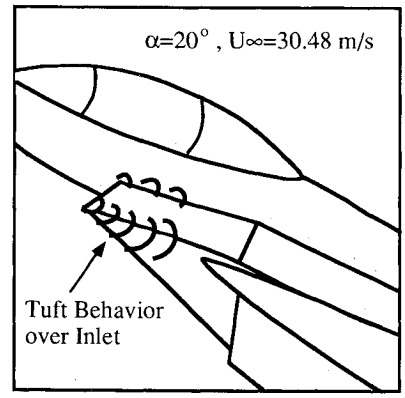

Fig. 6 Tuft behavior over the inlet, reconstructed from a digitized video image.

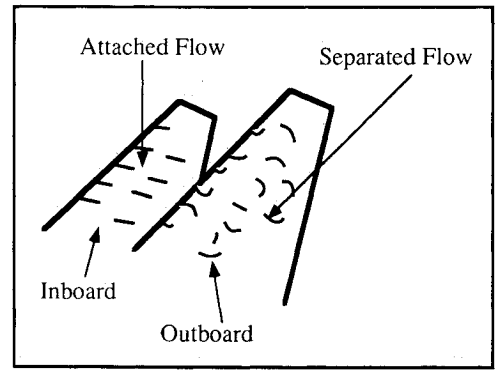

Fig. 7 Tuft behavior over the tail at α = 20 deg, reconstructed from digitized video images of the $\frac{1}{7}$-scale model.

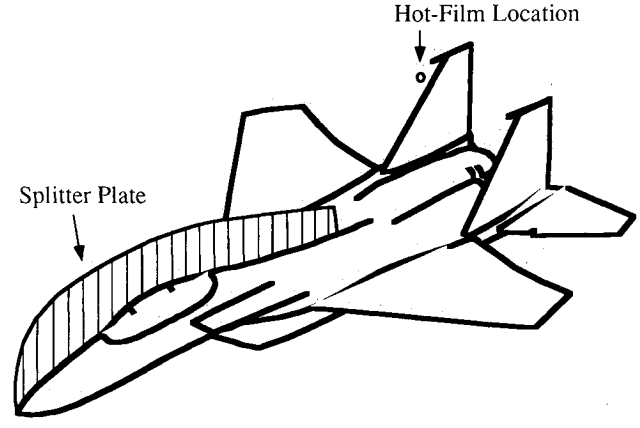

Fig. 8 Splitter plate experiment to check alternate vortex shedding effects on tail spectra.

interior is filled with a compound used in repairing automobile fenders. The engine ducts are left open. Inlet through-flow is varied using ejector nozzles or blockage inside the engine duct, and inlet droop is simulated. No stores are simulated. The only deviation from the aircraft geometry is that the vertical tail tip pods are removed to enable close approach to the tails with the laser velocimeter and hot-wire probes.

Initial laser sheet flow visualization tests were performed using a forked sting mount through the nozzles, connected to a three-axis computerized traverse system. For the LDV measurements, the mounting system was changed to that shown in Fig. 1 to minimize vibrations and support interference.[16] This system, built up from a camera tripod head, permits precise and rigid settings of model attitude as well as mounting the model in any of two positions to permit measurement of all three velocity components using a one-component LDV. The models are painted black to minimize laser scattering.

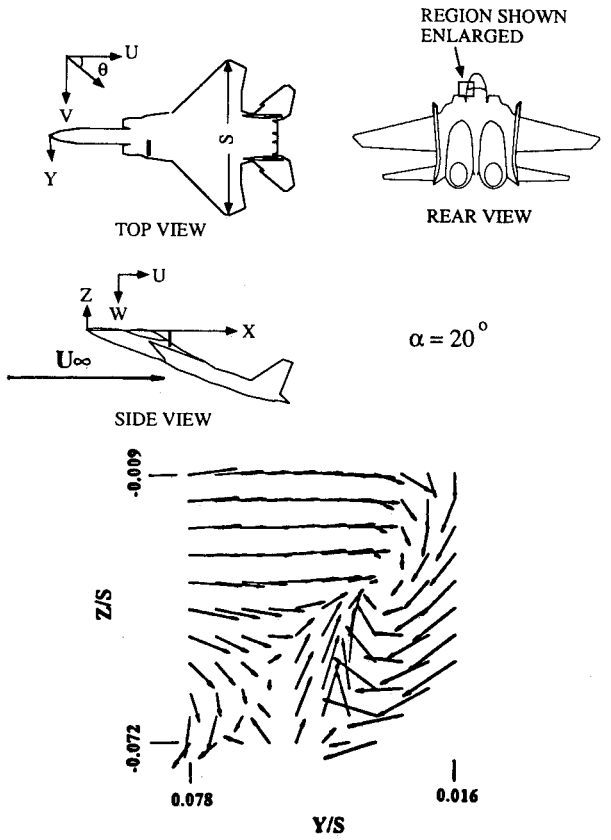

Fig. 9 Crossflow vectors above the gun bump (X/S = 0.563). The freestream velocity vector is shown for comparison.

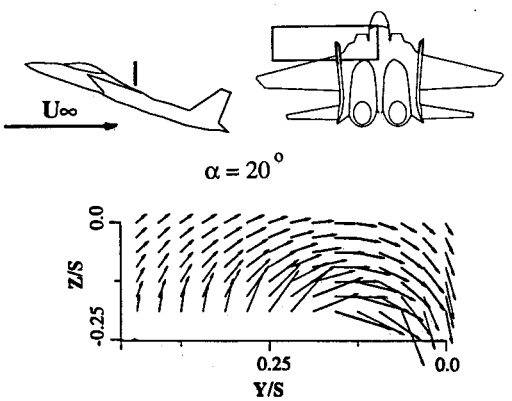

Fig. 10 Crossflow vectors above the wing (X/S = 0.8125). The freestream velocity vector is shown for comparison.

Fluorescent orange edges permit monitoring during LDV experiments performed with the test section darkened.

Wing surface co-ordinates near the leading edge were measured with displacement gauges, and compared with data used in computational fluid dynamics models of F-15 aircraft. The model wings were seen to be no thicker, and the leading edges no blunter, than the actual co-ordinates. Thus, at high angles of attack, wing flow separation lines should be located close to the leading edges on both the model and the full-scale aircraft.

Laser Sheet Videography

Figure 2 shows the arrangement for laser sheet flow visualization. An argon ion laser beam of approximately 3 W is expanded into a light sheet in the vertical plane. The sheet thickness is approximately the beam diameter: 1 mm. Two seeders located upstream provide scattered, random-path streams of low-speed air seeded with mineral oil droplets with a nominal droplet diameter of 5 μm. Thus, the entire flowfield

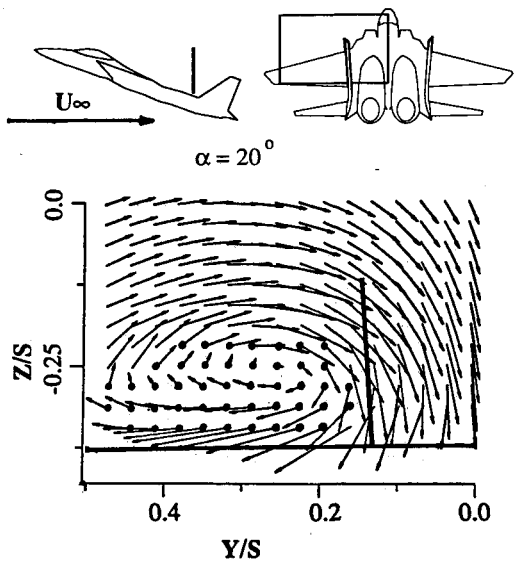

Fig. 11 Crossflow vectors upstream of the vertical tail (X/S = 1.125). The freestream velocity vector is shown for comparison.

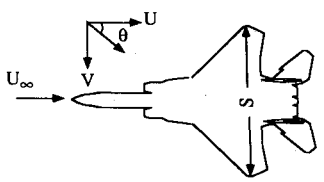

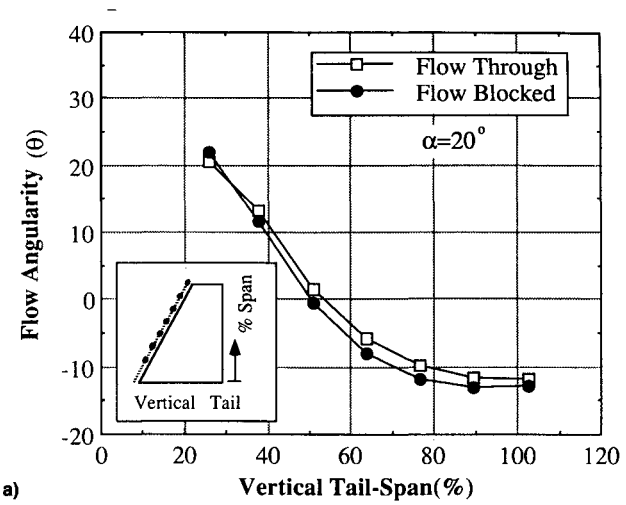

Fig. 12a Effect of inlet through-flow on flow angularity at the vertical tail.

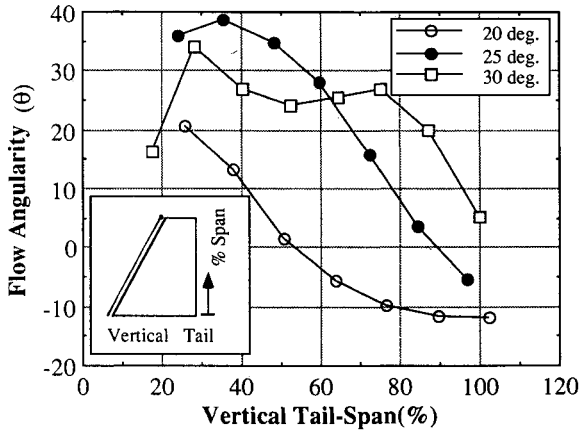

Fig. 12b Effect of angle of attack on flow angularity at the vertical tail.

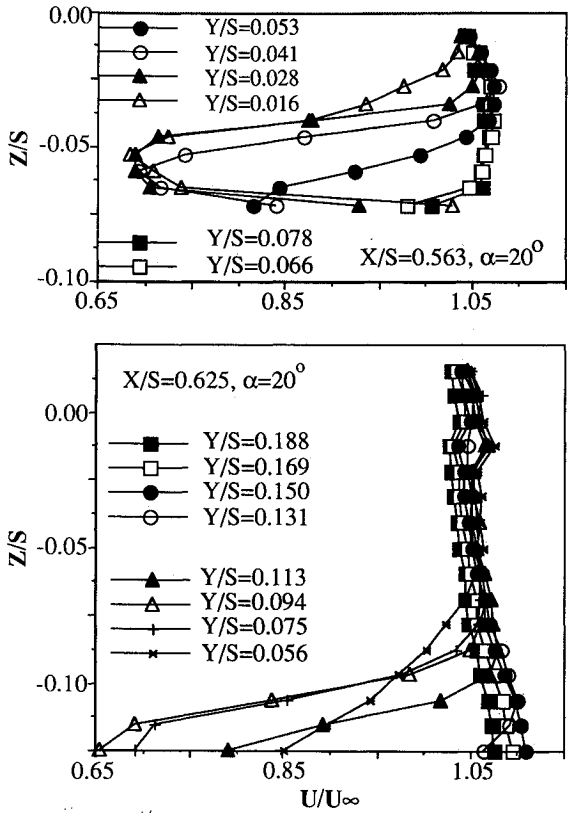

Fig. 13 Profiles of axial velocity across the vortex flow at several lateral stations and two longitudinal stations above the gun bump. U_∞ = 30.48 m/s, α = 20 deg.

over the model is seeded as opposed to the vortex cores alone. The model is moved longitudinally and vertically through the light sheet under computer control. Thus, the camera and the light sheet remain fixed, permitting accurate location of observed flow features. Initial video-recording of a poster board with a square grid enables scaling of the observed features.

Strong vortex cores are easily identified as regions in the light sheet devoid of light-scattering particles. This technique has been extensively used to document the trajectories of rotor tip vortices.[17] Thus, for example, the leading-edge extension vortices off a model of an F/A-18 are easily identified. In the F-15 flowfield, such strong vortices exist only in the vicinity of the canopy (forebody vortices) and downstream of the wing-tips at low angles of attack. The vortical flow over the rest of the model is observed more from the motion of the seeded flow, than from a stationary geometric pattern. This is qualitatively shown in Fig. 3. By careful observation of videotapes, it was possible to identify the centers of the vortical flow in each cross-sectional plane, and, thus, to track the trajectory of these centers. The flow visualization technique produces better visual results at low speeds. Some runs were made at higher speeds to check for changes in flow structure, and none were observed. For the trajectories presented below, the tunnel operating speed was approximately 5 m/s.

Laser Velocimetry

The LDV is powered by a 5-W Argon ion laser (usually operated at 3 W), with frequency shifters and a three-axis computerized traverse. The system, and previous applications to detailed time-varying rotorcraft flowfield diagnostics, have been described in Ref. 18. The traverse has a range of 48″ × 30″ × 30″, sufficient to cover the model. The LDV can be set up as a two-component system; however, this was considered to be an impediment to productivity in documenting the velocity field in this case. This decision precluded measurement of such quantities as a histogram of the resultant flow direction. Each component was measured separately. The

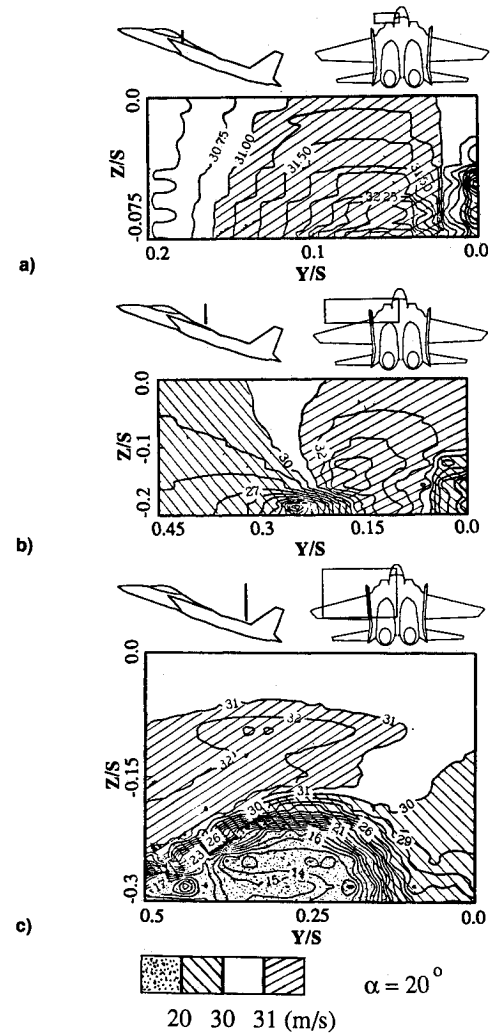

Fig. 14 Contours of u at the three crossflow planes. U_∞ = 30.48 m/s, α = 20 deg.

model was rolled 90 deg to measure the lateral component. Measurement planes were selected to define the flowfield near the inlets, over the wings, in front of the vertical tails, and across the vertical tails. Positional accuracy was essentially the same as the measuring volume size: approximately 0.1 mm at all points. This is achieved by linking the traverse system co-ordinates to fixed wind-tunnel coordinates before and after each run. The average data arrival rate per second varied from 200 in the more difficult regions near solid surfaces to 3000 in the freestream. The data rate was too low near the tail to permit spectral analysis of the velocity traces.

Results

Vortex Trajectories

Figure 4 shows two views of the vortex trajectories at α = 20 deg. The vortices originating from the forebody are clearly visible until they merge with the vortical flow over the inlets, and thereafter cannot be observed. Over the inlets, there is a roll-up of the flow, but no vortex core is observed. Further aft, the separated flow from the wing leading edge rolls up into a large vortical structure, and the inlet vortices soon become indistinct. The center of the vortical structure then moves outboard, and passes well outboard of the vertical tails. The elevation view shows that the trajectory is pulled down as it passes over the aircraft, and does not follow the freestream direction. The scatter in the data represent the precision with which these centers could be measured. No mean asymmetry is implied. Near the vertical plane of symmetry, there is strong downflow. At α = 30 deg, the flowfield is

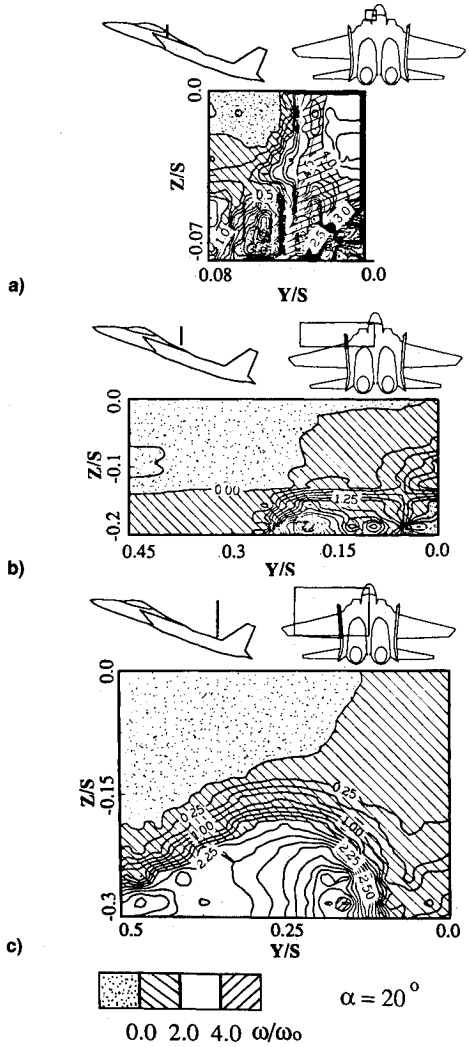

Fig. 15 Contours of the x-component of vorticity, normalized by ω_0 = 117.64 s^{-1} at the three crossflow planes: a) above the gun bump (X/S = 0.563); b) above the wing (X/S = 0.8125); and c) upstream of the vertical tail (X/S = 1.125).

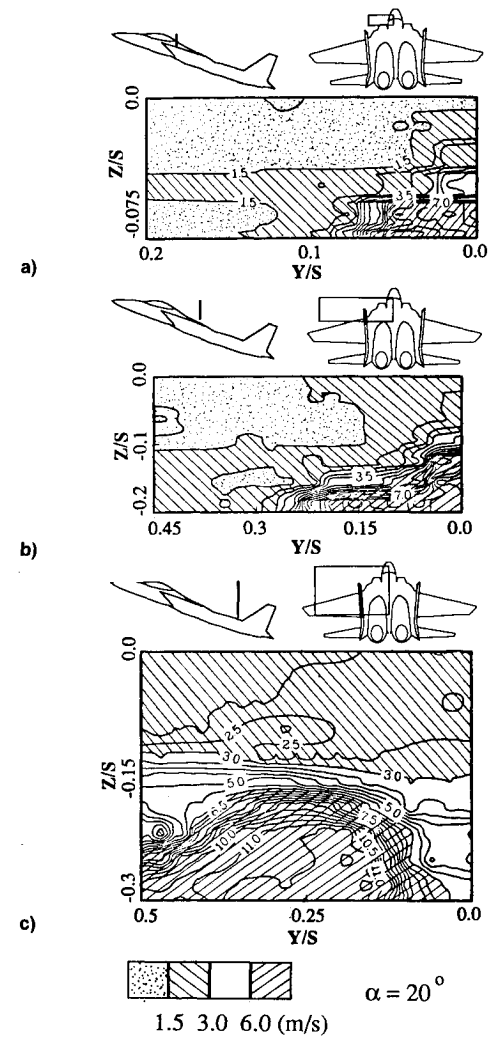

Fig. 16 Contours of root-mean-square velocity fluctuations at the three crossflow planes: a) above the gun bump (X/S = 0.563); b) above the wing (X/S = 0.8125); and c) upstream of the vertical tail (X/S = 1.125).

essentially similar, as seen in Fig. 5, except that the trajectory of the center of the vortical flow now passes the vertical tails at a higher position.

Surface Tuft Studies

The behavior of surface tufts was videorecorded for a range of flow conditions. These runs were made at a standard free-stream velocity of 30.48 m/s (100 ft/s). To study local flow behavior away from the surface, a single tuft on a wand was used. The angle of attack was changed in one-degree increments over the critical range from 10 to 23 deg, and in 2- or 5-deg intervals elsewhere, going from 5 to 30 deg. Continuous variations of angle of attack were also performed, in both directions. The analog video system was used for qualitative observation. A video-imaging system was used for more quantitative comparisons.

As α is increased from 5 deg, vortices emanate from the inlet leading edges, with counter-rotating structures from the inner and outer edges. This is reconstructed in Fig. 6, from a digitized video frame ($\frac{1}{60}$-s exposure) and is easily explained; the leading edges of the inlet act like sharp, swept-wing leading edges under spillage conditions. These vortices grow in intensity as α is increased, and merge with the strong roll-up over the "gun bump." Downstream of the wing midchord, only the massive vortical flow from the wing leading edge can be seen, so that the flowfield over the aircraft is characterized by just two large helical flow structures, one from each wing. The tufts on the wing surface become totally disorganized for $\alpha > 17$ deg, indicating total flow separation. The tufts near the vertical plane of symmetry remain organized and pointing slightly inward toward the plane of symmetry.

The behavior of the tufts on the vertical tail is especially interesting. As α is increased above 17 deg, flow separation propagates upward along the span of the vertical tail, on the outboard side. This continues until α = 20 deg, when the outboard sides are in fully separated flow. The tufts on this side are seen to be in violently agitated flow. Throughout this change, the tufts on the inboard sides of the tail remain relatively straight. The flow turbulence observed inboard is far less than that observed outboard. Figure 7 is reconstructed from the observations conducted on the $\frac{1}{7}$-scale model. These results differ somewhat from those reported in Ref. 1. There, separation reached the tip at 22 deg. The inboard side was reported to be in buffeting flow. The differences may be in the definition of buffeting flow. Here, the inboard tufts, though obviously in turbulent flow, did not exhibit flow recirculation except close to the leading edge, while the outboard ones flapped violently all over the tail surface.

Inlet Through-Flow and Droop

The tuft tests were repeated for varying amounts of through-flow in the inlet. The objective was to assess the significance of accurate through-flow simulation on studies of the tail buffet problem. The changes observed were too small to be considered significant, and these had to be studied more precisely using laser velocimetry. The effect of changing the inlet droop

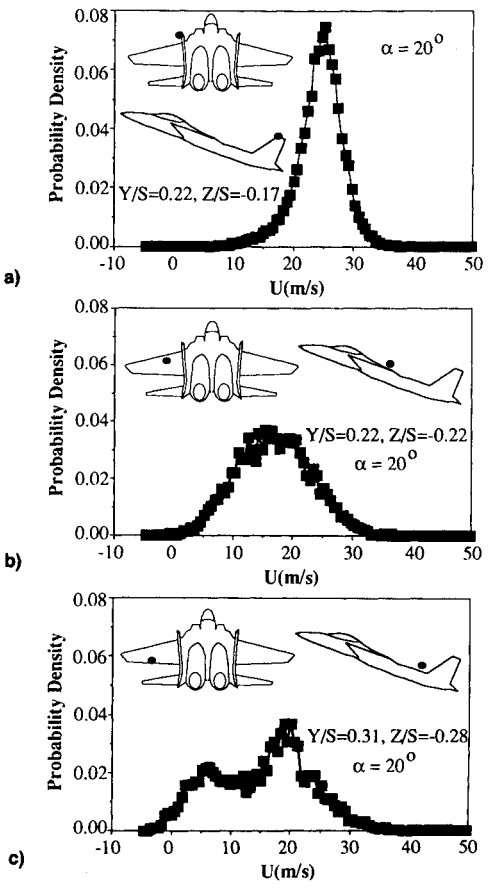

Fig. 17 Histograms of axial velocity: a) immediately upstream of the vertical tail leading edge; b) in the region of highest velocity fluctuations above the wing; and c) near the outboard edge of the vortex flow.

was studied by observing changes in tuft behavior. The strength of the inlet vortex was affected, but this produced no significant changes in the flowfield at the tail. Subsequent runs were conducted with the inlet drooped 11 deg.

Forebody Shedding Effects

The possibility of alternate vortex shedding from the forebody was checked by fixing a large thin splitter plate at the vertical plane of symmetry, extending from the nose to the wing midchord. The splitter plate was not extended to the tails for fear of inducing corner vortices at the tails. The configuration used is shown in Fig. 8. No effects were observed in the tuft behavior over the range of angles of attack tested, from 0 to 30 deg. Hot-film anemometer spectra were also measured near the leading edge of the vertical tail, with and without the splitter plate present, at $\alpha = 20$ deg. No significant effects were observed, and, hence, forebody shedding effects were not considered in the further studies of velocity fluctuations reported in Ref. 15.

Crossflow Vectors

All of the laser velocimeter data reported here were acquired at a freestream velocity of 30.48 m/s. Figure 9 shows crossflow velocity vectors in a rectangular region above the gun bump ($X/S = 0.5625$), at $\alpha = 20$ deg. The complexity of the vortex flow developing over the inlet and gun bump can be seen from this figure, along with the downflow generated by the forebody vortices. Over the wing ($X/S = 0.8125$), there is a clearly defined single vortex flow, as shown in Fig. 10. There is strong outflow near the wing surface. The cross-section at $X/S = 1.125$ includes the trailing edge of the wing and is just upstream of the vertical tails. The crossflow here is shown in Fig. 11. A clear vortical pattern is again evident, with high outboard-directed vectors near the wing surface. The core region appears to be elongated in the spanwise direction. The tails are seen to be immersed in this flowfield.

Flow Angularity at the Vertical Tail

One aspect of such a vortex flow is the development of large flow angularities at the leading edge of the vertical tail. In these experiments, this was explored using all three components of velocity at several points just upstream of the vertical tail leading edge. The time-averaged flow angles are large, and vary over a wide range, as seen from Fig. 12a. The presence or absence of flow through the inlet has only a small influence on this angularity, so that blocked-nozzle tests, where the inlet leading-edge geometry is properly modeled, should give fairly reliable results. However, as seen in Fig. 12b, the aircraft angle of attack has a large effect on this flow angularity. This flow angularity must cause complex steady loading patterns on the vertical tails, as well as local flow separation and unsteadiness. The instantaneous values of flow angularity, estimated using the histograms of the three components of velocity, take on much larger values. Thus, at the root, the time-averaged value is 24.3 deg. The instantaneous values range from -1.34 to $+59.7$ deg. At the tip, the time-average is -16.92 deg, while the instantaneous values range from -0.4 to -29.14 deg. Intermittent flow separation at the vertical tail surfaces seems inevitable.

These time-averaged values of flow angularity are comparable to those reported in Ref. 8, based on hot-film anemometry in the flowfield upstream of the vertical tails. There, the "sidewash" angle took on values ranging from about -14 deg (directed inboard) near the tip to 23 deg (directed outboard) near the root at $\alpha = 22$ deg on a 13%-scale model. The measuring planes were not the same, nor the angle of attack; thus, the closeness of actual values is fortuitous.

Axial Velocity Inside Vortical Flow

Profiles of axial velocity are plotted in Fig. 13 at several lateral (Y/S) stations across the vortex flow over the gun bump at two axial stations ($X/S = 0.5625$ and 0.625). The velocity deficit in the core also varies with angle of attack. The contours do show some regions, outside the core, where axial velocity is slightly above freestream values, but there was no substantial increase anywhere inside the core. Figure 14 shows contours of the u-component in the three cross-flow planes used in Fig. 9. Again, no increase is observed above freestream values. There is also no recirculation observed on a time-averaged basis: the u-component is not less than zero at any point studied. These features are quite different from those observed by Sellers et al.[9] in the vortex flow over the YF-17, where both acceleration and reverse flow were observed in the core region. Reversal of the instantaneous velocity does occur at several points in the flowfield. Points at which the histogram showed a substantial probability of reversal are indicated by darkened circles.

Vorticity Contours

Figure 15 shows contours of the x-component of vorticity in the cross-flow planes at $\alpha = 20$ deg. In Fig. 15a, there is a high concentration of vorticity generated over the inlet. In Fig. 15b, two centers of vorticity are visible: the stronger one is in the leading-edge vortex from the wing; however, the weaker vorticity from the inlet and gun bump is still discernible. In Fig. 15c, only one vortex center is seen. The region of strongest vorticity occurs surprisingly close to the fuselage, and is elongated in the vertical direction. Thus, despite the flattened appearance of the crossflow velocity vector plot for Fig. 15c, the vorticity appears to be concentrated closer to the fuselage.

Root-Mean-Square Velocity Fluctuations

Figure 16 presents contours of the root-mean-square velocity fluctuation above the aircraft at $\alpha = 20$ deg. The quantity plotted is the resultant $\{u'^2 + v'^2 + w'^2\}^{1/2}$. Again, strong fluctuations are seen in the highly vortical flow over the inlet.

In Fig. 16b, the fluctuations are strongest near the two centers of vorticity. The plot for Fig. 16c shows that the fluctuations are highest near the trailing edge of the wing surface, away from the region of strongest vorticity.

Histograms of Velocity Fluctuations

Intermittency of burst locations has been advanced as a source of fluctuations at the vertical tails of the F/A-18. Histograms of the velocity components were monitored to check for such effects on the F-15. Of special interest was the possible occurrence of bi-modal probability distributions of velocity. However, no such phenomena were observed near the vertical tails. The histogram at each location was constructed from 10,000 individual velocity values; the time to acquire these values varied from 10 s to 1 min, so that the sampling time was long enough to ensure statistical stationarity. Figure 17a shows the histogram of the u-component of velocity immediately upstream and outboard of the vertical tail. The distribution is sharp and smooth. The distribution in Fig. 17b, in the region of highest fluctuations above the wing surface, is much broader. No distinct bimodality is observed, but a broad range of axial velocity values can be seen. Figure 17c shows the distribution near the outboard edge of the vortex flow over the wings. Here, two peaks are evident, suggesting intermittency. This region is far outboard of any control surfaces, and is thus not relevant for the F-15.

Conclusions

The flowfield above a twin-tailed fighter aircraft model has been extensively documented using flow visualization and laser velocimetry. The following observations are made:

1. The concentrated vortices from the forebody merge into the vortex flow originating from the inlets, which in turn merges with the vortex flow from the gun bump and the wing leading edge.
2. Strong, unburst vortices are not observed downstream of the gun bump; the axial velocity profile shows a velocity defect in the core of the vortex flow.
3. The loci of the centers of the vortex flows move slightly inboard, and then outboard and downward, ending up well outboard of the vertical tails.
4. The vortex flow pattern causes a large variation in flow angularity at the vertical tail, which varies drastically with changes in aircraft angle of attack.
5. Inlet flow blockage seems to have only a marginal influence on the flow angularity at the vertical tail at angles of attack up to 25 deg.
6. The tuft studies show that flow separation and reversal propagate up the outside of the vertical tails with increasing angle of attack, but the flow on the inner surfaces of the verticals remains attached even at high angles of attack.
7. The time-averaged data do not show reversed flow over the wings; however, the instantaneous velocity does reverse at several points over the wings.
8. The root-mean-square intensity of velocity fluctuations is highest in the separated flow region immediately above the wing surfaces.
9. Bi-modal histograms of velocity are observed in the outer portion of the vortex flow over the aircraft, indicating violent fluctuations.

Acknowledgments

The authors gratefully acknowledge the assistance of Andrew Barr, undergraduate student, and Jae-Soo Hyun, Visiting Scholar, in acquiring some of the LDV data. This work was supported under a contract from the United States Air Force, Warner Robins Air Logistics Center. Dave Curry and W. Phillips are the Technical Monitors.

References

[1]Triplett, W. E., "Pressure Measurements on Twin Vertical Tails in Buffeting Flow," *Journal of Aircraft*, Vol. 20, No. 11, 1983, pp. 920–925.

[2]Wentz, W. H., "Vortex-Fin Interaction on a Fighter Aircraft," AIAA Paper 87-2474, Aug. 1987.

[3]Brandon, J. M., and Nguyen, L. T., "Experimental Study of Effects of Forebody Geometry on High Angle-of-Attack Stability," *Journal of Aircraft*, Vol. 25, No. 7, 1988, pp. 591–597.

[4]Reznick, S. G., and Flores, J., "Strake-Generated Vortex Interactions for a Fighter-Like Configuration," AIAA Paper 87-0589, Jan. 1987. See also, *Journal of Aircraft*, Vol. 26, No. 4, 1989, pp. 289–294.

[5]Schiff, L. B., Cummings, R. M., Sorenson, R. L., and Rizk, Y. M., "Numerical Simulation of High-Incidence Flow Over the F-18 Fuselage Forebody," AIAA Paper 89-0339, Jan. 1989.

[6]Ghaffari, F., Bates, B., Luckring, J., and Thomas, J., "Navier-Stokes Solutions about the F/A-18 Forebody-LEX Configuration," AIAA Paper 89-0338, Jan. 1989.

[7]Sankar, L. N., and Kwon, O. J., "Viscous Flow Simulation of Fighter Aircraft," AIAA Paper 91-0278, Jan. 1991.

[8]Colvin, B. J., Mullans, R. E., Paul, R. J., and Roos, H. N., "F-15 Vertical Tail Vibration Investigations," McDonnel Aircraft Co., St. Louis, MO, MDC Rept. A6114. Sept. 1979.

[9]Sellers, W. L., Meyers, J. F., and Hepner, T. E., "LDV Surveys Over a Fighter Model at Moderate to High Angles of Attack," Society of Automotive Engineers TP Series Paper 88-1448, Oct. 1988.

[10]Zimmerman, N. H., Ferman, M. A., Yurkovich, R. N., and Gerstenkorn, G., "Prediction of Tail Buffet Loads for Design Applications," AIAA Paper 89-1378-CP, 1989.

[11]Del Frate, J. H., and Zuniga, F. A., "In-Flight Flow Field Analysis on the NASA F-18 High Alpha Research Vehicle With Comparisons to Ground Facility Data," AIAA Paper 90-0231, Jan. 1990.

[12]Erickson, G. E., Hall, R. M., Banks, D. W., Del-Frate, J. H., Schreiner, J. A., Hanley, R. J., and Pulley, C. T., "Experimental Investigation of the F/A-18 Vortex Flows at Subsonic Through Transonic Speeds," AIAA Paper 89-2222, 1989.

[13]Schrader, K. F., Reynolds, G. A., and Novak, C. J., "Effects of Mach Number and Reynolds Number on Leading-Edge Vortices at High Angle of Attack," AIAA Paper 88-0172, Jan. 1988.

[14]Edwards, J. W., "Assessment of Computational Prediction of Tail Buffeting," NASA TM 101613, Jan. 1990.

[15]Komerath, N. M., Schwartz, R. J., and Kim, J. M., "Flow Over a Twin-Tailed Aircraft at Angle of Attack. Part II: Temporal Characteristics," Submitted to *Journal of Aircraft*.

[16]Ericsson, L. E., "Reflections Regarding Recent Rotary Rig Results," *Journal of Aircraft*, Vol. 24, No. 1, 1987, pp. 25–30.

[17]Brand, A. G., Komerath, N. M., and McMahon, H. M., "Results from the Laser Sheet Visualization of an Incompressible Vortex Wake," *Journal of Aircraft*, Vol. 26, No. 5, 1989, pp. 438–443.

[18]Liou, S. G., Komerath, N. M., McMahon, H. M., "Velocity Measurements of Airframe Effects on a Rotor in Low-Speed Forward Flight," *Journal of Aircraft*, Vol. 26, No. 4, 1989, pp. 340–348.